

Total Lightning Mapping using both VHF Interferometry and Time-of-Arrival Techniques

Jean-Yves Lojou, *Vaisala SAS - Marseille, France*

Kenneth L. Cummins, *Dept. of Atmos. Sciences, University of Arizona / Vaisala Inc. - Tucson, USA*

Abstract— As part of Vaisala’s technology and applications test bed in the Dallas-Fort Worth area in Texas, we have been operating two overlapping total lightning detection networks. One is based on the VHF Interferometry principle while the other is based on the VHF Time-of-Arrival principle. For the first time, these two technologies can be compared in a common region where they both exhibit good performance. The aim of the work presented in this paper is to evaluate the performance of these networks and compare the relative strengths of these two approaches for Total Lightning mapping.

Index Terms— Cloud discharge, Coverage, Interferometry, Storm Cell, Time-of-Arrival, Total Lightning, VHF.

I. INTRODUCTION

Lightning discharges are comprised of several processes that radiate in different manners. Intermittent VHF emissions that propagate with velocities in the range of 10^5 m/s tend to occur during virgin breakdown and stepped leader processes, whereas more-continuous emissions propagating above 10^7 m/s occur during K changes and dart leaders in established channels [1-3]. The large current variations associated with return strokes in cloud-to-ground lightning are mainly observable in the low frequency (LF) spectrum [4]. In this paper we focus on the VHF emissions produced by lightning and techniques to locate them.

The characteristics of VHF lightning emissions range from single very short pulses lasting a few microseconds to continuous emissions lasting over several milliseconds, as illustrated in Figure 1.

Different detection and localization methods are best suited to the different radiation patterns. Intermittent or isolated pulses are best suited to time-of-arrival techniques where each sensor reports the precise arrival time of the largest VHF emission in short (~ 100 μ s) time intervals. The location is then deduced from the analysis of time-of-arrival differences among sensors [4-5]. For a three-dimensional (3D) time-of-arrival location system, the minimum number of sensors required is four. Typical distances between sensors, to allow accurate data reconstruction, are in the range of 10-40 km. In most cases, such networks are composed of 7 to 12 sensors.

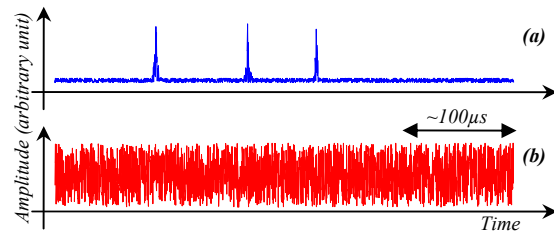


Fig. 1. Typical VHF radiations: a) very short single pulses, well adapted to timing-based location methods (LDAR) and b) very long (up to several milliseconds) continuous emissions, well suited to interferometry-based location methods.

Long-duration VHF emissions with little amplitude modulation are well suited for interferometry. Each sensor consists of an array of closely-spaced dipoles arranged in a way to produce the direction-of-arrival (azimuth) of the source by employing phase differences between pairs of dipoles, typically integrated over 10’s of μ s. It is also possible to obtain 3D locations using interferometry by deriving an elevation angle using special antenna arrangements [6-7]. The source location is then obtained by computing the triangulation of the azimuth and/or elevation from at least 2 sensors [8]. For such networks, the typical distance between sensors is in the range of 50-150 km, and they are composed of at least 3 sensors.

The categorization of the two techniques presented above is somewhat of a simplification in order to present the basic concepts. In fact, time-of-arrival networks are also able to locate multi-pulse events or even continuous emission as long as there is sufficient modulation of the amplitude to allow a precise time stamping of the events. Similarly, interferometric networks are able to operate on short pulses as long as the integrated signal level over the acquisition period is large enough to ensure a sufficient signal/noise ratio.

There are longstanding questions regarding the relative ability of these two techniques to depict the spatial and temporal behavior of individual lightning flashes and thunderstorms (Mazur et al., 1997). In an effort to help resolve these open questions, Vaisala has recently deployed four interferometric sensors to augment the VHF time-of-arrival test bed in the Dallas-Fort Worth (DFW) Texas area [9]. For the first time, these two types of networks have overlapping coverage such that they

both have good performance for the same thunderstorms. The aim of the work presented in this paper is to evaluate the performance of these networks and to compare the relative strengths of these two approaches for total (CG plus cloud) lightning mapping.

Vaisala's Texas Test Bed is composed of an LDAR II network, a "medley" Interferometric network (two LS8000, one 2D SAFIR and one 3D SAFIR), and it uses CG data from the U.S. National Lightning Detection Network™ (NLDN). Figure 2 shows the configuration of the two VHF networks.

The geometry of the VHF Interferometric network is a triangle with sensor spacing of about 100 km around the Dallas-Fort Worth area. One original SAFIR sensor is installed at the southwest corner (Granbury), a 3D SAFIR sensor is located on the northwest corner (Decatur) and two prototypes of the recently released LS8000 sensor complete the network to the east (Mesquite and Plano). Having these two very close sensors does not significantly improve the network performance (detection efficiency or location accuracy), but it has been useful for

qualifying the new generation LS8000 sensors. All four interferometric sensors are shown as light blue disks in Figure 2.

The VHF Time-Of-Arrival network is composed of seven LDAR II sensors, with one sensor at the DFW airport and six others arranged to best cover the DFW urban area (plain symbols in Figure 2). The distance between nearest sensors ranges from 20 to 30 km. The optimal zone of detection is identified by a white circle in Figure 2.

These two datasets are complemented by the cloud-to-ground (CG) flash data produced by the National Lightning Detection Network™ (NLDN). In the area of interest, the CG flash detection efficiency is approximately 95%, with a median location accuracy better than 500m. This has been validated against video observations of lightning [10].



Fig. 2. Vaisala Texas Test Bed is made of 4 VHF Interferometric sensors (blue circled symbols) and 7 VHF time-of-arrival ones (plain symbols) in the Dallas-Fort Worth area. The white circle (about 80 km radius) indicates the optimal zone of detection of the Time-of-Arrival network.

II. OBSERVATIONS AND ANALYSIS

This analysis employs data from thunderstorms in the

DFW area during July and August, 2005. We first evaluate the detection efficiency (DE) of the VHF networks for CG flashes located by the NLDN, and

compare them with simulations. Since the in-cloud component of CG flashes generally occurs at lower altitudes than their counterparts in cloud flashes, this serves as a “worst case” analysis of detection efficiency for total lightning. We then focus on the ability of these systems to describe the spatial and temporal characteristics of cells/storms through an analysis of a particular storm occurring on July 1st. Finally we explore the ability of each system to describe the spatial and temporal characteristics of individual flashes, providing a representative example and presenting calculated velocity distributions for the within-flash processes, derived from all flashes occurring during the test period.

A. Detection Efficiency

The DE was determined using CG flashes reported by the NLDN as a ground truth. VHF systems do not directly measure return strokes of CG flashes, but they do detect other associated discharges that occur as part of a CG flash. Thus, a VHF network was said to have detected a CG flash reported by the NLDN if it located at least one source within 30 km of the first stroke location, within ± 300 ms. A simple count of such events divided by the actual number of CG flashes within a grid box of 5x5 km provided the estimates of DE.

Figure 3 shows the DE of the time-of-arrival network with optimum detection directly over the sensor array, and a rapid decrease in DE with increasing distance. The decrease with distance is more rapid than most other VHF time-of-arrival networks, due to somewhat higher receiver noise, and the fact that the network operates with reduced sensitivity in order to be able to operate in real time.

Figure 4 shows the same map for the interferometric network. The 90% DE contour derived from the simulation has been superimposed (solid black contour). There is very good agreement between the observation and the simulation. For the simulated DE, we have assumed that the VHF sources were centered at a height of 4000 m. We employed a complete propagation model including terrain blockage, 0.1° diffraction at the radio horizon, and an effective earth radius scaled up by 4/3 to take into account refraction effects. We assumed that the source power followed a Gaussian distribution centered on +36 dBm with 5 dB standard deviation.

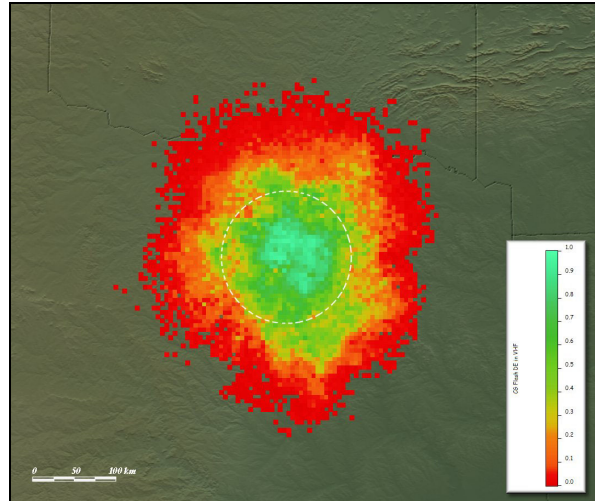


Fig. 3. Time-of-Arrival network detection efficiency of CG lightning. Dashed circle indicates the high DE region of the LDAR II network during the period of this study.

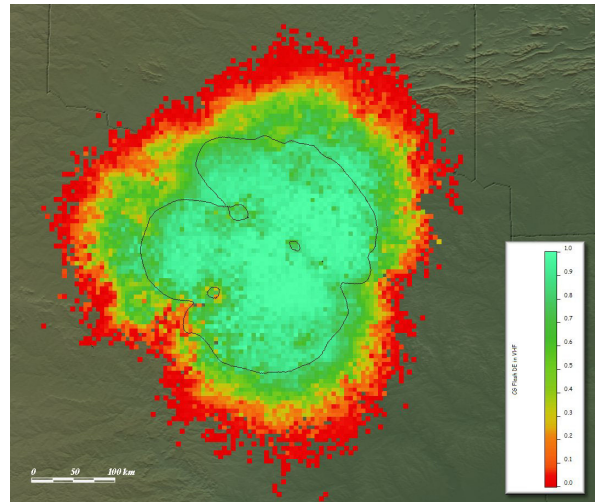


Fig. 4. Interferometric network detection efficiency of CG lightning. The solid black line corresponds to 90% detection efficiency of the flashes located at an altitude of 4000m.

This analysis clearly shows that the Interferometric network covers a larger area with fewer sensors than the Time-of-Arrival network.

B. Flash Rates

In order to compare the functional performance of the systems, we evaluated several thunderstorms and analyzed the flash rate over the lifecycle of the storms. Figure 5 is a chronographic map of one representative storm situation on July 1, 2005 that exhibited an interesting behavior. This storm was composed of two main cells that moved independently from north to south, and then merged over the Dallas-Fort Worth urban area, just before dissipating. The dashed circle in this figure represents the high DE region for the LDAR II network.

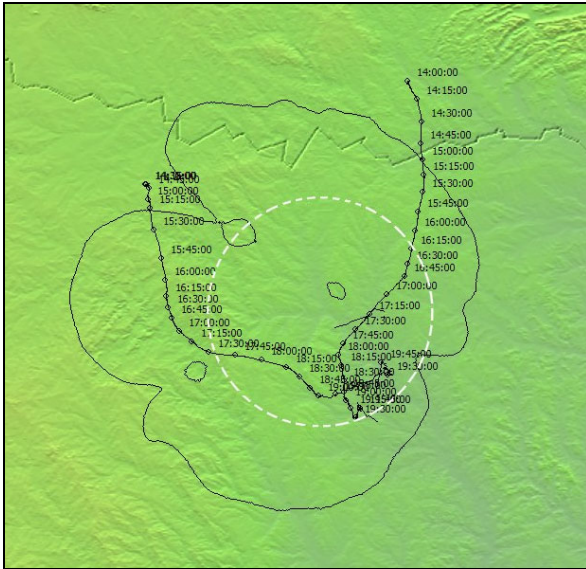


Fig. 5. Cell tracks of the July 1st, 2005 thunderstorms over the Dallas-Fort Worth area. Two main cells were traveling from north to south and merged just before dissipating. Cells are time-stamped every 15 minutes. No cell merging algorithm was applied in this processing leading to an erratic path at the end of the southwest cell track.

To produce this image, we employed a cell tracking algorithm specifically designed to operate on continuously-arriving lightning data. For each new detected event, being either a CG return stroke or a VHF “source” cloud event, we first determine if the sample can be associated with an existing cell. This association is made using a “gravity” function based on the flash density. If an association is made, the position and other parameters of the cell are updated taking into account the weighted positions of all events constituting the cell. If not, the sample is placed in a “pool” that is periodically checked to determine if local flash density exceeds a given threshold in order to start a new cell. Given the greater range of the interferometric network, its data were used to produce the cell tracks in Figure 5.

This algorithm is able to update the position of the cells very frequently, to produce an estimate of the cell motion and growth, and to accumulate many parameters. Examples are CG flash rate, cloud flash rate, and (when available) radar parameters including max reflectivity, precipitation, etc. The version of the cell tracking algorithm used in this example has no cell merging or splitting capability. This allowed us to track individually the two cells, but it also resulted in an erratic path for the southwest cell when the two cells merged.

Figure 6 shows the time trend of the flash rates (VHF time-of-arrival and VHF interferometry cloud flashes, as well as positive and negative CG flashes) for the northwest cell, derived using the cell tracking algorithm.

Once this cell was within the detection area for both networks (16:15 UTC), the cloud flash rates became very similar, showing the same shape and approximately the same rate. We also note a small precedence (leading by

about 10 minutes) for the time-of-arrival rate, starting at about 17:00 UTC.

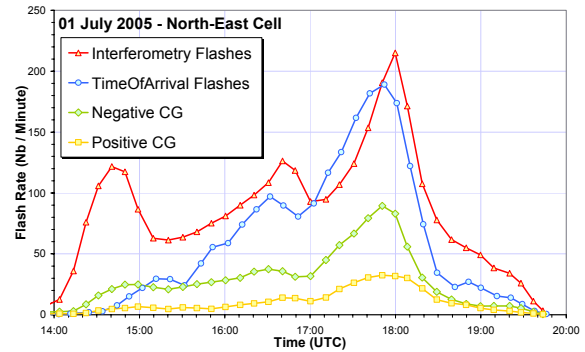


Fig. 6. Flash rate of one of the two cells constituting the thunderstorms that occurred July 1st, 2005 over the Dallas-Fort Worth area. Once the cell is in the detection area of the LDAR II network (after 16:00 UTC), both VHF systems provide about the same number of flashes. Positive CG lightning reaches its maximum rate when the cell starts to dissipate at 18:00 UTC.

For the southwest cell (see Figure 7), the number of flashes detected by the LDAR II network is about half of the value detected by the interferometric network. This is simply due to the fact that this cell traveled outside the optimal detection area of the Time-Of-Arrival network until after 18:00 UTC, as shown in Figure 3.

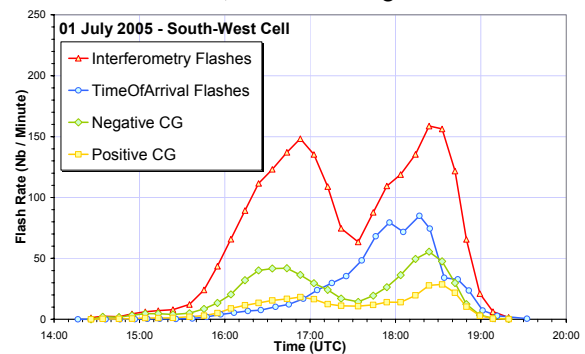


Fig. 7. Flash rate of the other cell constituting the thunderstorms that occurred July 1st, 2005 over the Dallas-Fort Worth area. For this particular cell the VHF interferometry gives a higher number of flashes, even in the high DE region for the time-of-arrival system, and shows a very good correlation with the negative CG counts (3 times higher however). As in the previous cell, positive CG rate is at its maximum as the cell starts to dissipate at about 18:30 UTC.

The second increase in flash rate, after 18:30 UTC, is due to a side effect of the cell merging occurring approximately at this time. For both cells, there is a good correlation between the CG and cloud flashes rates, with an almost constant ratio of 3:1 for the IC:CG ratio.

C. Flash Extent Density

Since a cloud flash observed by VHF techniques is made up of hundreds to thousands of sources with individual (point) locations, we apply a branching algorithm to “connect all the dots” that comprise a flash. We then build the flash extent density (FED) which provides density (flash count per unit area per unit time)

of flashes in each grid box traversed by these branches [11]. The FED is less sensitive to the source DE than a simple source density, and will also reflect the actual number and spatial extent of the flashes, hence the name.

Figure 8a shows the FED for the two-cell storm situation on July 1st, 2005 obtained with the data acquired by the VHF Interferometric network.

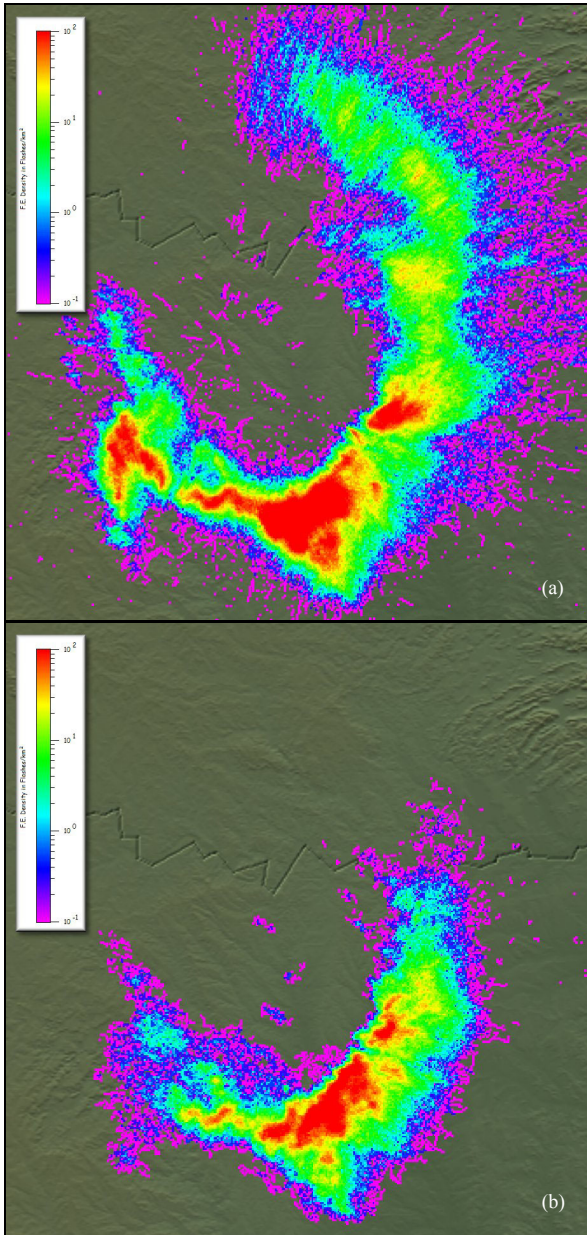


Fig. 8. Flash extent density as measured by the VHF networks on July 1st, 2005 over Dallas area: (a) by interferometry; (b) by time-of-arrival technique.

This representation clearly illustrates the spatial extent of the cells. Both show a “width” of about 70 km, although the southwest cell has a finer structure with two parallel tracks about 20 km in width. A large

intensification (brighter image) of the FED is also clearly noticeable at the time the two cells merge.

Figure 8b shows the FED representation for the Time-Of-Arrival network. This figure shows the same features as Figure 8a, confirming the ability of both techniques to describe the lightning activity at a cell and storm level.

The CG FED obtained from the NLDN data is provided in Figure 9. It illustrates the lower density of CG flashes compared to the cloud flashes. Since CG information provides only one sample per return stroke, it also provides a poorer description of the spatial extent of the storm. Where the southwest cell is divided in two segments, the most northern path produces almost no CG activity, and would be very difficult to track in the absence of cloud discharge information.

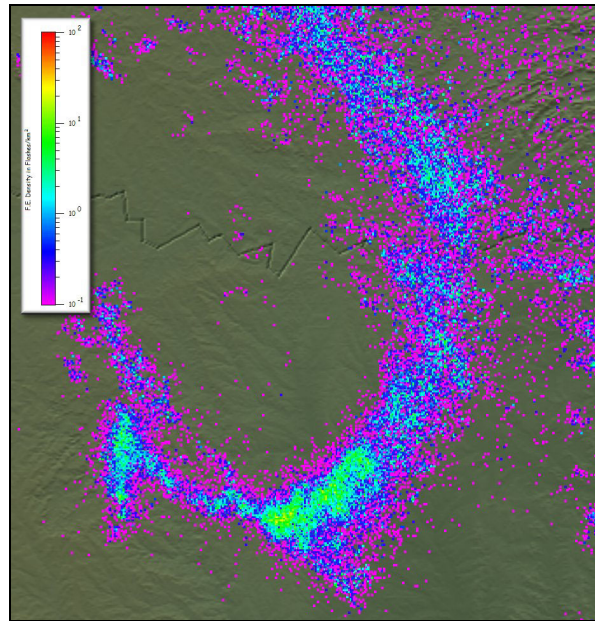


Fig. 9. Cloud-to-ground flash density as measured by the NLDN on July 1st, 2005 over Dallas area.

D. Total Lightning Representation

The previous section illustrated the good correlation between the two VHF detection techniques over the lifecycle of two single-cell storms. In this section we isolate the total lightning activity during the mature phase of a small multi-cellular complex that is moving to the southeast (Figure 10). This display technique depicts the lightning branches from cloud discharges as well as the CG locations. The most recent CG strokes (i.e. occurring over the last minute) are coded as bright white dots showing the current position of the lightning cell cores. The past 30 minutes of CG flashes are coded as + or – red symbols according to polarity. Current cloud flashes (most recent minute) are represented with their branches in green, and the branches occurring in the past 30 minutes are shown in blue.

This display technique clearly illustrates the beginning of a trailing stratiform region forming on the trailing side

of the storm. This region extends from the cores of the cells where the highest density of CG flashes occurs (bright white area) toward the northwest. Note the isolated positive CG flash during the most-recent minute that occurs 30 km backward in this trailing stratiform region (see arrow in Figure 5(a)) In the absence of the “context” provided by total lightning mapping, one would not know if this CG flash was the beginning of another cell, an isolated flash in an electrified stratiform region, or a badly located CG flash.

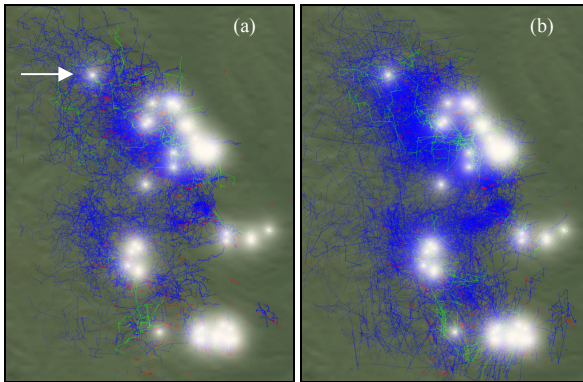


Fig. 10. Branch representation for VHF time-of-arrival (a) and interferometry (b) for lightning activity occurring between 14:48 and 15:18 UTC July 7th, 2005. The most recent CG strokes are coded as bright white dots showing the current position of the lightning cell cores. The past 30 minutes of CG flashes are coded as + or - red symbols according to polarity. Current cloud flashes (most recent minute) are represented with their branches in green, and the branches occurring in the past 30 minutes are shown in blue.

Both VHF detection techniques provide a very comprehensive way to identify such a CG threat in areas where the rate and the density of CG flashes may be low while the cloud flash rate stays at a high level.

E. Flash Representation

In order to explore the finer-scale differences between the two VHF technologies, we look at the representation of individual flashes.

Significant differences are well illustrated in the time:elevation representation of a cloud flash, shown in Figure 11. Due to the location of this flash relative to the position of the observing (Decatur) interferometric sensor, a 10° elevation reported by the interferometer corresponds to about 14 km above ground. This figure illustrates two clear differences between the two techniques. First, interferometry shows the presence of very fast moving (very short time intervals) vertically-oriented bursts of emissions, related to dart leaders or recoil streamers in established channels (see up-pointing arrows in Figure 11). Second, the VHF time-of-arrival technique provides a dense representation of long-duration horizontal branches (X in Figure 11), likely composed of very narrow pulses resulting from negative breakdown in a positive charge region. Although interferometry is not well suited for such pulse-like events, some of them are also located by this system.

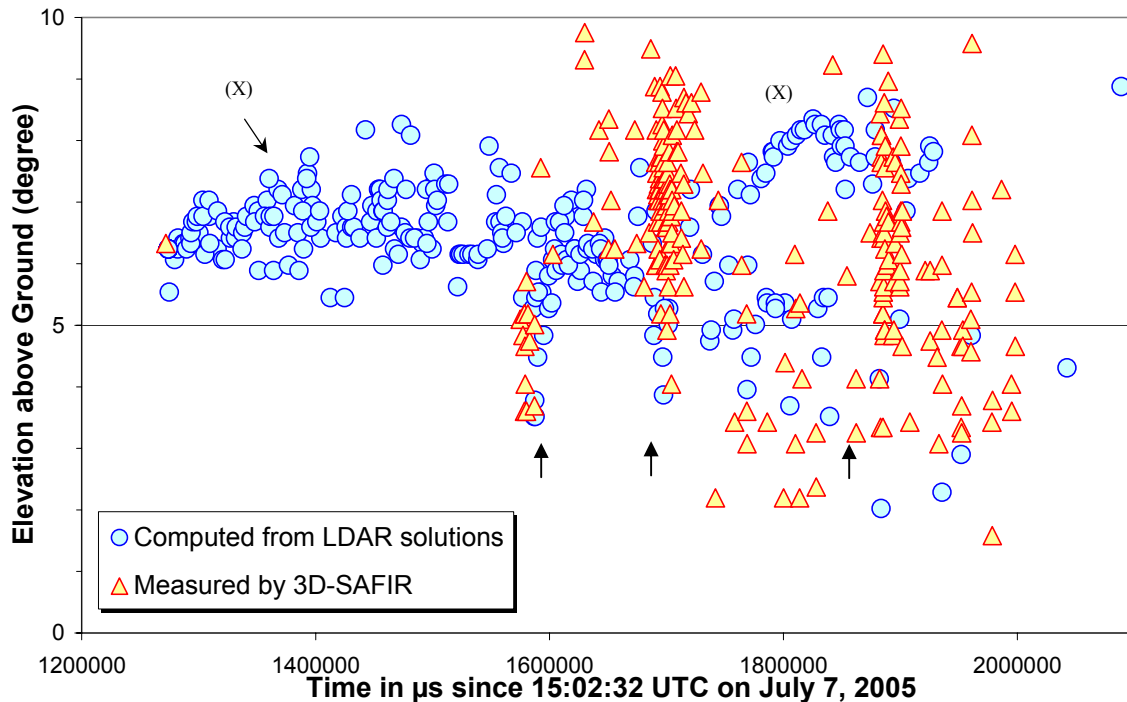


Fig. 11. Time series of the elevation above ground as seen from the Decatur 3D VHF interferometer (triangles) and the VHF Time-of-Arrival network (circles). Unlike time-of-arrival, interferometry exhibits “bursts” of vertical emissions (arrows) separated by 100 to 200 ms. The VHF time-of-arrival technique is more suitable for long duration, slow propagating, branches (X sign).

Although the bursts of emissions measured by interferometry appear, at this time scale, to have a very short duration, they actually occur during about 20 ms, which is long enough for such technology. On the other hand, the long duration horizontal branches detected by time-of-arrival appear to be continuous, whereas the average time separation between samples is 10ms.

The two-dimensional shape and extent of this flash, as seen from above, is shown in Figure 12. The white flash representation is for interferometry and the black representation is for time-of-arrival. The colors surrounding each branch reflect time-of-occurrence (see legend).

Although the branches (derived from a best-guess connection of the located sources) do not match well, the general position and extent of the two flash representations are quite similar. This similarity was expected, based the FED plots seen in Section II.C. The

differences seen at the detailed level at least partially reflect the complementary nature of the two measurement techniques that is clearly illustrated in the time:height plot in Figure 11.

Figure 13 is another example of such a time:height plot, for a negative CG flash. This is a 10 stroke flash with a very high current first stroke (-85 kA). Almost all strokes (located by the NLDN and depicted by green vertical lines) are time-coincident with a rapid sequence of VHF emissions, seen most-easily by the Decatur interferometer. This is consistent with the fact that interferometry is best suited to detect fast moving, almost continuous bursts like those that occur in the leader processes of CG strokes. The Time-of-Arrival network also detected a few VHF sources for many of the strokes, but is better at representing horizontal breakdown that occurred as part of charge reorganization at the end of the flash. The interferometer produced a few sources at the extreme end of the flash.

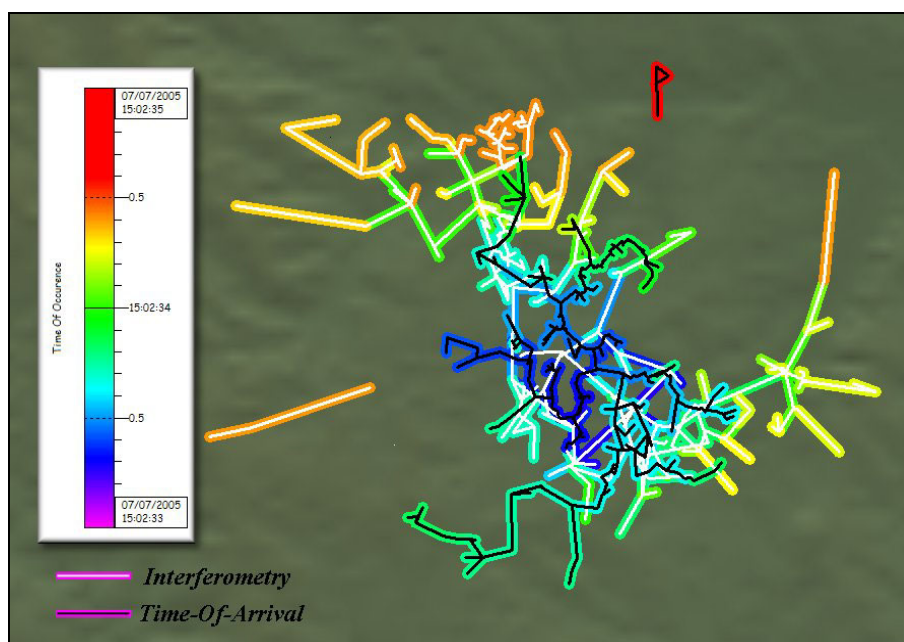


Fig. 12. 2D plots of the same cloud flash (July 7th, 2005 15:02:33 UTC) located by VHF interferometry (light path) and time-of-arrival (dark path).

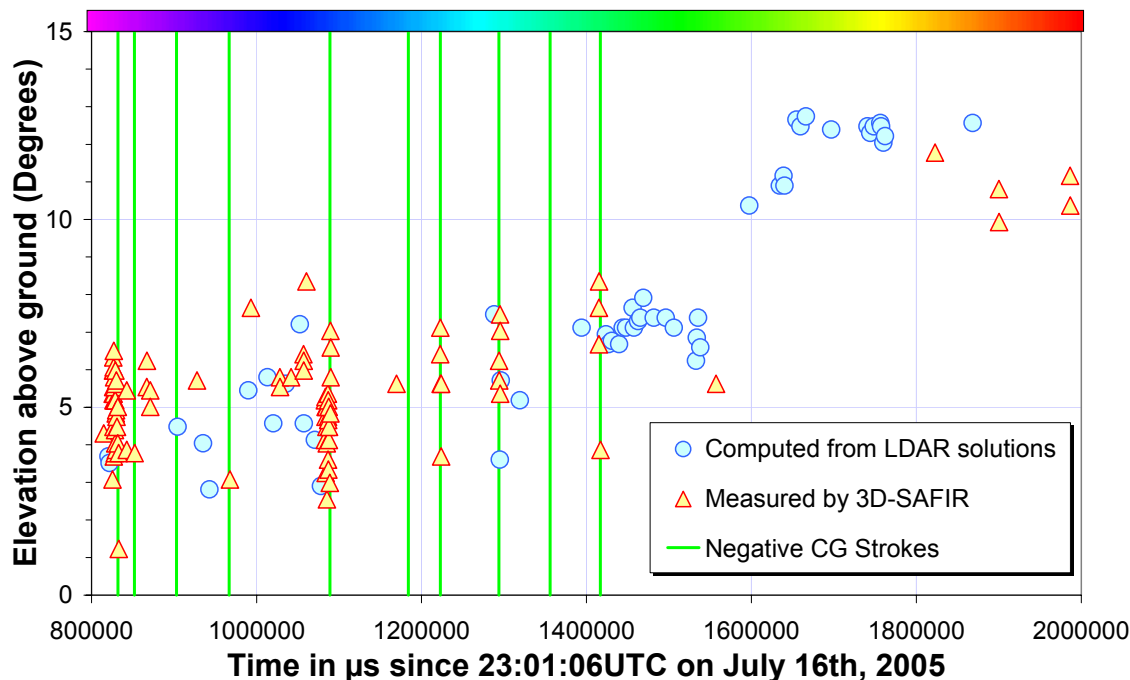


Fig. 13. Time series of the elevation above ground as seen from the Decatur 3D VHF interferometer (triangles) and the VHF Time-Of-Arrival network (circles). Vertical green lines represent the occurrence of the CG strokes.

A 3D representation of this CG flash is given in Figure 14. This figure corresponds to the data acquired by the Time-of-Arrival network (blue circles in Figure 13). Even though the flash appears to be a single continuous branch, the analysis of the time series in Fig. 13 shows that it is made of several different processes that occur during the life-cycle of the CG flash. According to the rainbow color scale on top of Figure 13, the green to orange portion of the path is truly a single branch propagating upward in the cloud but, the purple to blue portion is the result of the interconnection between some “undersampled” events of the different leader:stroke sequences.

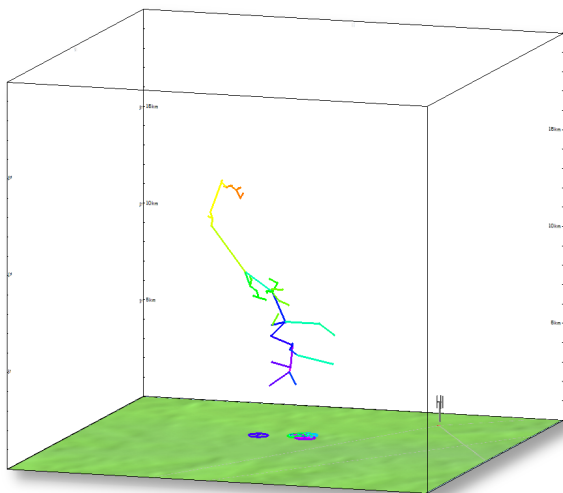


Fig. 14. 3D representation of CG a flash, recorded by the Time-Of-Arrival network, occurring July 16th, 23:01:06 UTC. The flash is color coded according to the time of the locations from purple to orange (see rainbow scale on top of Fig. 13)

To conclude this study, we evaluated the distribution of the propagation velocity along the flash branches, as shown in Figure 15. These distributions have been obtained for all flashes acquired during July and August 2005.

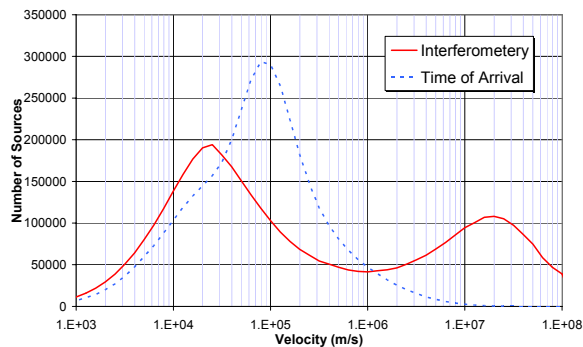


Fig. 15 Distribution of the velocity of the branches for VHF interferometry (solid line) and VHF time-of-arrival (dashed line). VHF interferometry shows a bimodal distribution with a collection of fast events (bursts) with velocities centered at 2×10^7 m/s (not seen by time-of-arrival), and a second mode centered at 2×10^4 m/s, also noticeable on the time-of-arrival distribution. The peak of velocity for VHF time-of-arrival is at 10^5 m/ where interferometry did not significantly contribute.

Velocities for discharges reported using interferometry show a clear bimodal distribution with a first population of events propagating at a velocity of about 2×10^7 m/s and a second one at about 2×10^4 m/s. The fast events

correspond to the quasi-continuous emissions (very short time separation between samples) while the lower-velocity population is due to a mixture of effects. Some reflect the temporally isolated samples in the slow branches, such as the ones marked by an (X) in Figure 10, whereas others reflect an “apparent propagation” (spatial and temporal separation) between two bursts of the same flash, typically separated by 100-200 ms. The velocity distribution for VHF time-of-arrival is unimodal with a peak at approximately 10^5 m/s, which is consistent with existing literature (Mazur et al., 1997).

III. DISCUSSION AND CONCLUSION

Based on observations obtained during Summer 2005, we have shown that VHF Interferometric networks can cover a larger area with fewer sensors than 3D VHF Time-of-Arrival systems. We note that this wider sensor spacing has the side effect of poorer source location accuracy – approximately one km, as compared to 100 m for VHF time-of-arrival. From the FED analysis, we have shown that both techniques can provide a complete general representation of the two-dimensional spatial and temporal characteristics of cells and storms, including counts of flashes. This study also confirms the greater “richness” and spatial continuity of the total lightning mapping data provided by both VHF networks, when compared to a “CG-only” lightning detection system. The poorer location accuracy for interferometry does not appear to compromise the FED description of storms. From a practical point of view, VHF time-of-arrival sensors offer the advantage of being easier to install, with less constraint on the environment (close obstacles, size of installation area). Moreover VHF time-of-arrival systems can inherently provide 3D solutions, whereas VHF interferometry must employ large and/or complex antenna arrangements in order to provide 3D information. Another benefit of VHF time-of-arrival is ease of detecting extremely narrow (sub-microsecond) pulses.

This complementary nature of the two VHF technologies is clearly reflected in the detailed spatial and temporal evolution of individual flashes. It is clear that VHF time-of-arrival provides a more complete representation of the three-dimensional time evolution of a flash, but interferometry provides information about important processes not well-represented by time-of-arrival data.

In conclusion, it appears that both techniques are capable of providing similar and complete descriptions of

two-dimensional total lightning activity at the cell and storm scales, but they provide complementary information at the level of individual flashes.

ACKNOWLEDGEMENT

The authors wish to acknowledge all of their colleagues who contributed to the success to this work – both past and present (Brad Bilbrey, John Cramer, Nick Demetriades, Ron Holle, Marjorie Ilpide, Geoffroy Mortreux, Martin Murphy, Joe Nowak, Mike Pezze, Andre Soulage, Vincent Tremosa and Randy Wasser)

IV. REFERENCES

- [1] Mazur V., P.R. Krehbiel, X.M. Shao, Correlated high-speed video and radio interferometric observations of a cloud-to-ground lightning flash, *J. Geophys. Res.*, 100, D12, 25,731-25,753, 1995.
- [2] Shao, X.M., P.R. Krehbiel, The temporal development of intracloud lightning, *J. Geophys. Res.*, 101, D21, 26,641-26,668, 1996.
- [3] Mazur, V., E. Williams, R. Boldi, L. Maier, D.E. Proctor, Initial comparison of lightning mapping with operational Time-of-Arrival and interferometric systems, *J. Geophys. Res.*, 102, D10, 11,071-11,085, 1997.
- [4] Cummins, K.L., M.J. Murphy, J.V. Tuel, Lightning detection methods and meteorological applications. Presented at the IV International Symposium on Military Meteorology, Malbork, Poland, September 25-28, 85-100, 2000.
- [5] Thomas, R. J., P. R. Krehbiel, W. Rison, S. J. Hunyady, W. P. Winn, T. Hamlin, and J. Harlin (2004), Accuracy of the Lightning Mapping Array, *J. Geophys. Res.*, 109, D14207, doi:10.1029/2004JD004549.
- [6] Defer, E., P. Blanchet, C. Thery, P. Laroche, J.E. Dye, M. Venticinque, K.L. Cummins, Lightning activity for the July 10, 1996, storm during the Stratosphere-Troposphere Experiment: Radiation, Aerosol, and Ozone-A (STERAO-A) experiment, *J. Geophys. Res.*, 106, D10, 10,151-10,172, 2001.
- [7] Meng Qing, Zhang Yijun, HePing, Xu Xiaofeng, ZhaoJunzhuang Philippe Rouquier, Jean-Yves Lojou, Lightning Observation and Field Experiment with 3D SAFIR System during Summer 2003 in Beijing-Hebei Area, presented at the 27th International Conference on Lightning Protection, 13-16 September 2004, Avignon - France
- [8] Richard, P., A. Delannoy, G. Labaune, P. Laroche, Results of spatial and temporal characterization of the VHF-UHF radiation of lightning, *J. Geophys. Res.*, 91, 1248-1260, 1896.
- [9] Demetriades, N.W.S., M.J. Murphy, MJ, Cummins, KL: Early results from the Global Atmospheric, Inc. Dallas-Fort Worth Lightning Detection and Ranging (LDAR-II) research network. AMS, Sixth Symposium on Integrated Observing Systems, 13-17 January 2002, Orlando, Florida.
- [10] Kehoe K., Krider E.P., NLDN Performance in Arizona, 18th International Lightning Detection Conference, Tucson, AZ, 2004.
- [11] Lojou, J.Y., K. L. Cummins, On the representation of 2D and 3D Total Lightning Information, presented at the 1st Conference on Meteorological Applications of Lightning Data, 85th AMS Annual Meeting – San Diego, USA, 2005.